Operational Features of a Linear Slit Colloid Microthruster

Julius Perel and John F. Mahoney
Phrasor Scientific Incorporated
Duarte, CA 91010
Phone: (626) 357-3201
jperel@phrasor.com
IEPC –01-116

A prototype microthruster design has been developed which is capable of delivering thrust over the range 1-30 micro-Newtons, using the technology of electrohydrodynamic emission of multiply charged microclusters, termed colloid propulsion. Historically, colloid thruster emitters have been tested based on three design configurations: needle-like capillaries[1], annuli[2] and slit geometries[3]. We are developing a microthruster design using the linear slit geometry which is more robust than capillary needle arrays and easier to fabricate compared to either capillary or annuli geometries. Design features of these linear slits are compatible with micromachining technology and therefore adaptable for MEMs microminiaturization of future thruster systems.

Slit Blade Bodies

The linear slit design, shown in Fig.1 includes a photochemically etched "rake" sandwiched between two 1/8" thick slit bodies, each tapering to provide blade edges of 25 micron thickness. The "rake" substrate includes a propellant delivery plenum, flow impedance channels and fingers for anchoring charged microcluster emission sites. Each slit body is machined from heat treatable 440C stainless steel. The machined blades are then heat treated to a Rockwell C hardness of 55 in vacuum (˜100 mtorr) at 1700-1800 °F (service provided by Supreme Steel Treating, Inc. So. El Monte, Ca.). Hardened blade material is required to prevent slit edge "roll-up" and to preserve surface flatness during subsequent lapping/polishing stages. The propellant wetted inner blade surfaces (facing the "rake") are ground and polished using a succession of alumina grinding discs starting with 30µ stepping down to 9µ abrasive material. After grinding, the surfaces are polished using a 1µ alumina suspension. In addition to maintaining surface planarity, the foregoing fabrication procedure allows a metal-to-metal rake/blade sealing capability after the assembly is compressed using a bolt assembly. As a further precaution, slit structural seams can be electron or laser beam welded to guard against any propellant

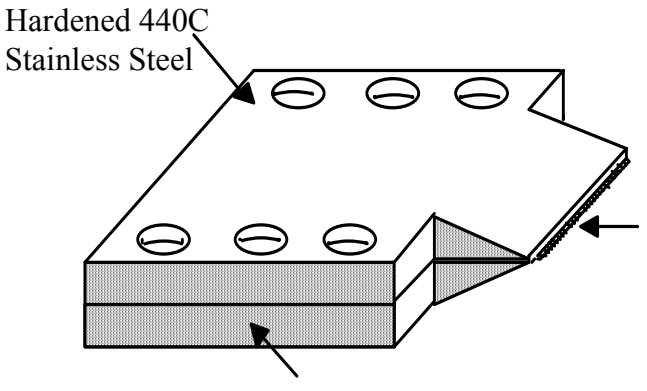

Fig. 1 Microthruster linear slit geometry

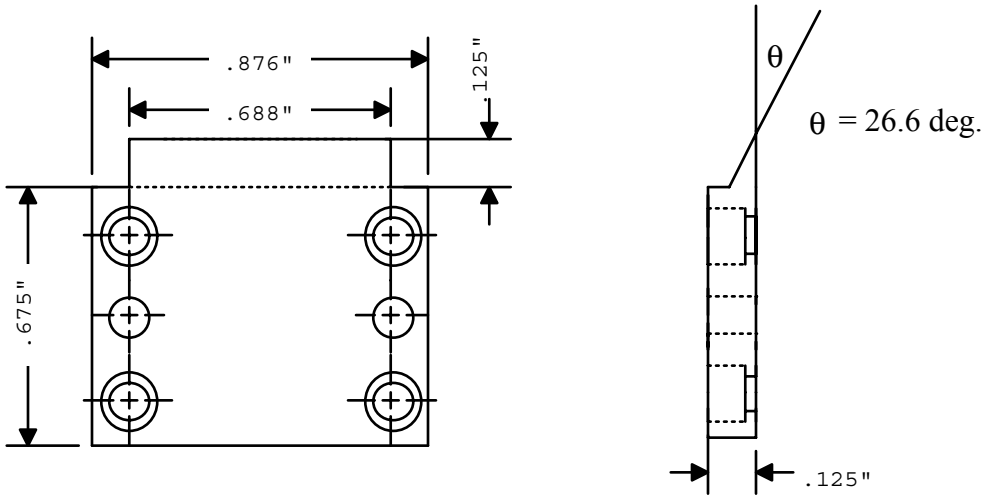

Fig. 2 Linear slit body dimensions (shown on 2:1 scale).

leakage. Preliminary tests have shown the metal-to-metal seal to be satisfactory. The dimensions of the two identical slit bodies used in the prototype configuration are shown in Fig.2.

The design of the rake substrate placed between the slit bodies determines the thrust range achievable by the microthruster. An advantage of this assembly is that rake substrates designed for different thrust ranges are interchangeable and can be used with the same linear slit body.

Rake Substrate Design

A photochemically etched rake configured for assembly between the two slit blades is shown in Fig.3. The rake substrate has a thickness of 75μ. A number of flow grooves, 50μ deep, are etched into the rake body. The grooves serve to deliver propellant from a filled plenum to the emission end of the slit containing a number of fingers separated by gaps. Prototype rake substrates are manufactured by United Western Enterprises, Inc. located in Camarillo, Ca. During assembly, the emission end of the rake is positioned to protrude a few mils (˜ 0.004 inches) from the end of the blade tips. This exposes the emission sites to the high fields (> 10^5 V/cm) formed in the region separating the slit and extraction electrode. A simple method used for determining rake design elements is given below with the aid of Fig.4.

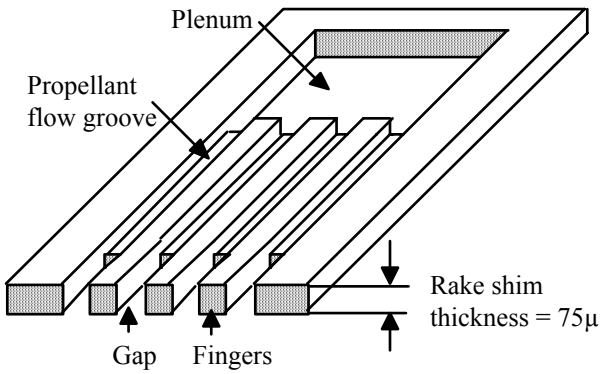

Fig. 3. Photochemically etched rake (shim) concept.

.

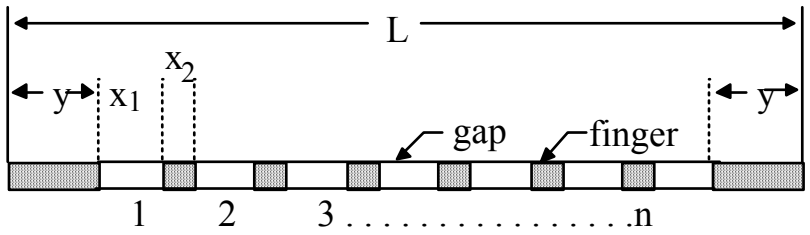

Fig.4 Linear slit rake design elements.

The number of rake fingers (emission anchor sites) can be computed from

$n - 1 = [(L + x_2 - 2y)/(x_1 + x_2)] - 1$ ("n" must be an integer)

where:

n-1 = number of rake fingers
n = number of gaps
L = total length of rake
y = length of end wings
x_1 = gap separation
x_2 = length of rake finger

The above expression will be used to calculate initial test rake substrate dimensions and also any design modifications necessary to achieve the 1-20 μN thrust range.

The rake substrate is the most important element in the design of a linear slit microthruster and serves several functions:

a The rake provides a means for introducing propellant flow uniformly to the flow grooves.

b. It provides a controllable high flow impedance geometry.

c. It is anticipated that the shim will provide a means for anchoring emission sites for spatial and temporal stability.

Two photochemically etched rake configurations (version A and B) were designed, fabricated and tested during this report period. In Fig. 5, only a few rake fingers and gaps are shown for clarity. Both rake configurations consisted of 58 gaps and 57 fingers. The first rake tested (version A) pointed out some design weaknesses and was replaced with version B. Three significant changes were introduced into the slit rake design for version B.

a. The 50μ deep propellant flow channels were lengthened from 0.5 to 0.6 inches to increase the flow impedance.

b. The length of the protruding rake fingers were shortened from 0.125 to 0.02 inch.

c. Mounting tabs were added to the photochemically etched rake structure for ease of alignment during microthruster assembly.

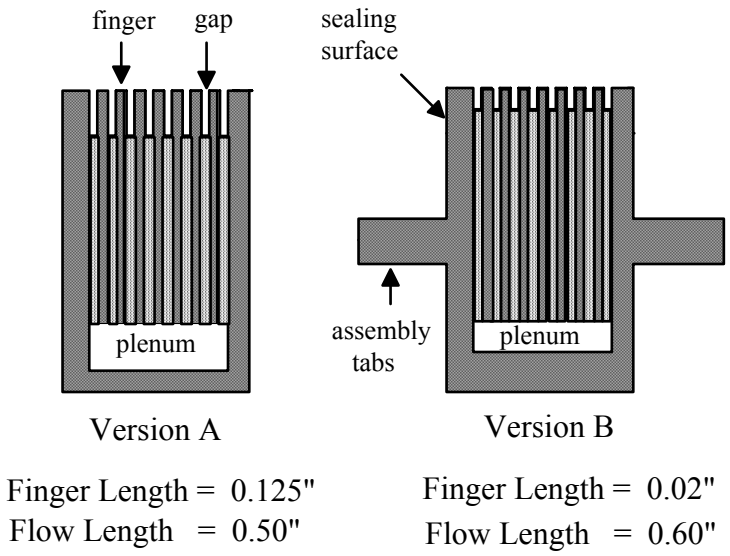

Fig. 5. Photochemically etched rake configurations.

Linear Slit Microthruster Performance

Fig.6 shows an assembled linear slit microthruster enclosed by an insulating Delrin housing ready for mounting in a test chamber. The extractor electrode for the linear slit consists of two 0.063 inch dia. polished stainless steel cylindrical rods spaced 0.130 inches apart. The rectangular electrode seen in Fig. 6 serves as an electron suppresser element and is typically operated at -250 volts, connected electrically to the extractor electrode at the same potential. The electron suppresser electrode is necessary in ground-based tests to prevent electrons, which originate from chamber surfaces bombarded by the microcluster beam, from impinging on microthruster elements held at high, positive acceleration potentials. Fig. 7 shows a schematic of the test apparatus for measuring the current-voltage performance of the colloid microthruster. Current-voltage plots of the colloid microthruster using the version B rake are displayed in Fig. 8. Two experimental I-V curves are shown in the figure; one for the microthruster operating with surface tension feed of the propellant and one showing the I-V performance when the glycerol propellant (1.4M NaI) is delivered under a positive pressure of 1 atmosphere. The lower currents measured for the micro-thruster operated by atmospheric pressure feed, over the voltage range of interest, appears counterintuitive. At these high flow rates, large droplets are emitted carrying a large positive charge, but having a low charge-to-mass ratio. Under these flow conditions, the microthruster emission current would be limited, dominated by space-charge effects. On the other hand, under surface tension feed, smaller droplets are emitted with higher charge-to-mass ratios. Also, the smaller droplets are emitted at much higher frequencies and launch velocities.

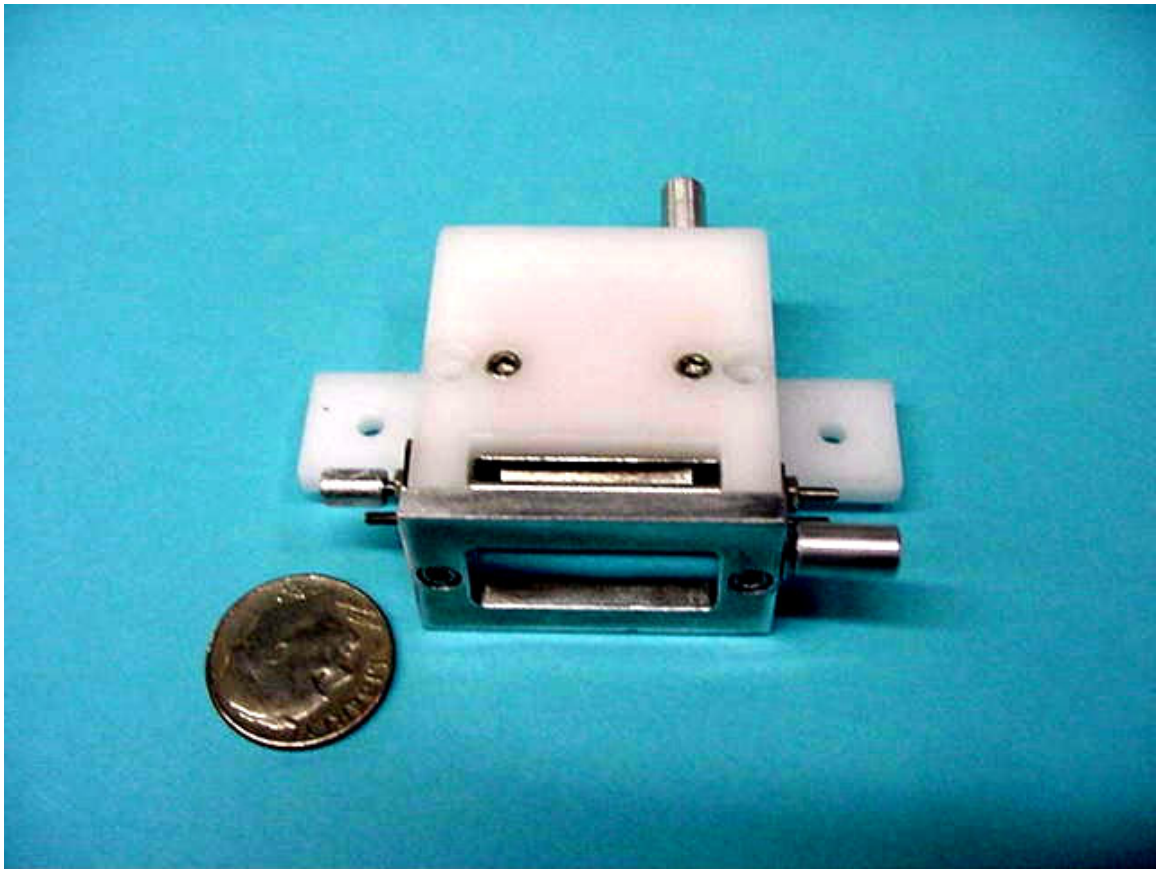

Fig.6 Assembled linear slit colloid microthruster

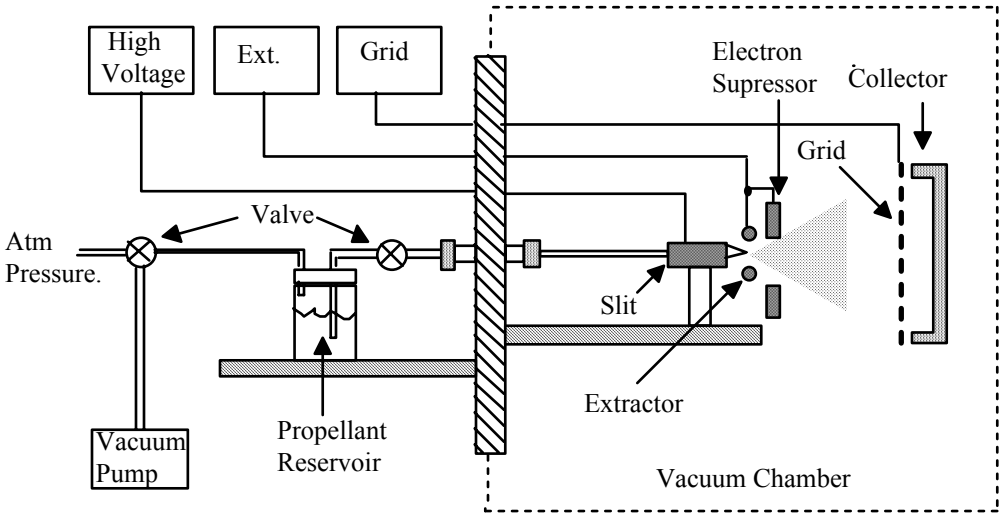

Fig. 7. Colloid microthruster test apparatus.

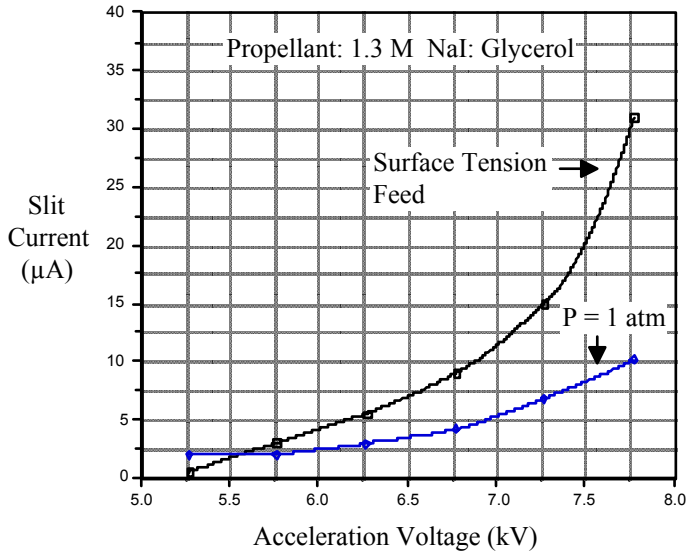

Fig. 8 Linear slit microthruster current-voltage performance.

The Child-Langmuir space-charge law states that the emission current I is given by

$$I = K\,(q/m)^{1/2}\,V^{3/2} \qquad (1)$$

where V is the acceleration potential, indicating that particles with high charge-to-mass ratios (q/m) result in higher currents. Table 1 summarizes the thrust and specific impulse performance of the linear slit colloid microthruster operated under capillary feed conditions.

The performance in Table 1 is based on calculated mass flow rates, dm/dt, assuming propellant flow is governed by electrostatic pressure only. Using the calculated value for the propellant flow rate and experimentally determined values for the emitted current, the mean value of the charge-to-mass ratio was obtained from

$$\langle q/m \rangle = I/(dm/dt) \qquad (2)$$

The mean microcluster velocity was then found using $\langle v \rangle = [2\langle q/m \rangle V]^{1/2}$, where V is the potential applied to the emitter, allowing thrust and specific impulse estimates using $T = \langle v \rangle (dm/dt)$ and $I_{sp} = \langle v \rangle / g$ where g is the acceleration due to gravity.

Table 1. Colloid microthruster performance using capillary feed.

Current (μA)	Voltage (kV)	Specific Impulse (sec)	Thrust (μN)
0.5	5.27	164	3.3
3.0	5.77	400	8.9
5.5	6.27	520	13.6
9.0	6.77	635	19.5
15.0	7.27	796	28.0
31.0	7.77	1,110	44.0

Theoretical Predictions

After closer examination of the I-V characteristics for the case of capillary fed propellant (see Fig.8), there appears to be an anomalous jump in the emission current at about +7.50 kV, a phenomenon which is repeatable based on several measurements. At this voltage, the emission current appears to double from the previous voltage setting. The I-V dependence prior to this setting (up to 7.25 kV) follows a space-charge limited dependence according to the relation

$$I = K (V - V_o)^{3/2} \qquad (3)$$

where K is a constant determined from the experimental data and V_o is the onset voltage where emission begins. Fig. 9 shows the close fit of the experimental data to eq.3 starting from the onset voltage up to V = 7.25 kV. At this point a deviation from the space-charge dependence is observed.

The deviation observed is possibly due to a change in the number of emission sites controlled by the geometry of the rake fingers. Since the emission current was observed to nearly double at the transition voltage, it is postulated that the number if emission sites also doubled at the transition voltage. This

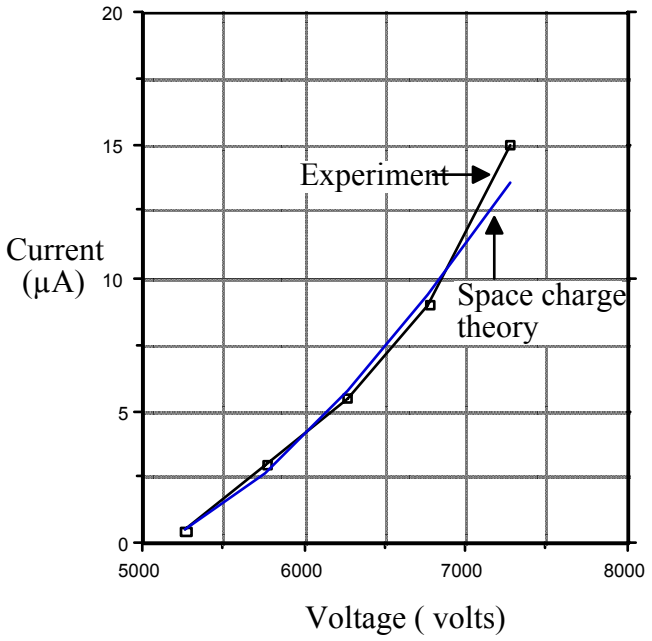

Fig. 9. Microthruster space-charge limited operation.

scenario is depicted is Fig.10. Here we postulate that the emission cusps at onset up to the transition voltage are anchored at alternate rake sites. (Alternatively, the emission sites could be anchored over the gaps between the rake fingers). Once the transition voltage is reached, the number of emission cusps can double by forming over each rake finger element. If this is verified by future experimental studies, then it would appear that the geometrical rake structure does indeed anchor and add stability to the emission sites over absence of the rakes. In the figure, λ_r is the fixed, as-fabricated, wavelength or spacing between the rake fingers. The following analysis lends support to the concept of cusp doubling when the electric field at the slit reaches the critical transition value.

When a thin liquid layer of a non-viscous, conducting fluid is subjected to an electric field E applied normal to the surface, small perturbations grow which evolve into cusps separated by a characteristic wavelength, λ . The following dispersion relation can be used for the analysis of cusps formed along a linear slit geometry[4]:

$$\omega^2 = (k/\rho) (\rho g - \varepsilon_o E^2 k + \gamma k^2) \qquad (4)$$

where ρ and γ are the fluid density and surface tension; g is the acceleration due to gravity; ε_o is the permittivity of free space = 8.85×10^{-12} F/m; and E is the electric field intensity in the region above the cusps.

For small wavelength disturbances, the liquid surface tension provides the dominant restoring force and the gravity term in eq.4 can be neglected. Solving the above for the wave velocity $v = \omega / k$ gives

$$v = \omega / k = (1/\rho)^{1/2} (\gamma k - \varepsilon_o E^2)^{1/2} \qquad (5)$$

Assuming the cusps formed along the linear slit remain fixed, i.e., the wave velocity is zero, yields $(\gamma k - \varepsilon_o E^2)^{1/2} = 0$

Solving the above for E (using $k = 2\pi/\lambda$) provides a relationship showing the dependence of cusp wavelength on the electric field strength,

$$E = (2\pi\gamma / \varepsilon_o \lambda)^{1/2} \qquad (6)$$

The electric field for a linear slit can be given as

$$E = V / (2rR)^{1/2}$$

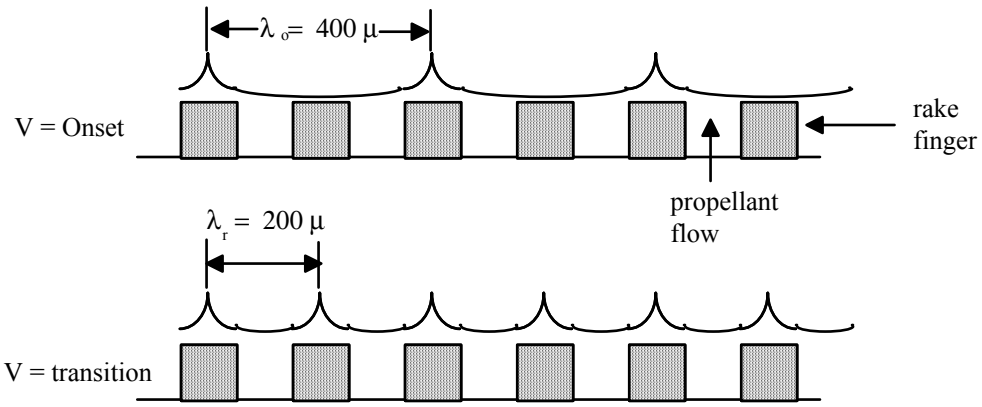

Fig. 10 Linear slit emission site dependence on applied voltage.

where V is the voltage applied to the slit, r is the radius of the slit (rake) edge and R is distance to the extractor electrode. Setting eq. 7 equal to eq. 6, an expression is obtained relating the cusp wavelength to the voltage applied to the linear slit,

$$\lambda = (4\pi\gamma\, rR/\varepsilon_o)(1/V^2) \qquad (8)$$

For glycerol with γ = .063 N/m, r =.0015" and R = 0.130", refer to Table 2.

Note that the analysis predicts that a cusp wavelength of about 400 microns is predicted near the onset voltage. Furthermore, the analysis predicts a decrease in the onset wavelength to 200 microns (equal to the characteristic rake wavelength) at about the transition voltage observed experimentally. Here the number of emitting cusps can double explaining the factor of two increase in the emission current. It should be noted that the transition effects discussed above were observed for two different linear colloid microthrusters.

Neutralization

One of the advantages of colloid micro-propulsion devices is that spacecraft neutralization can be achieved by bipolar operation. Bipolar operation basically requires the simultaneous emission of positive and negative colloid beams. The advantage of

Table 2. Cusp wavelength dependence on applied voltage.

	Voltage (volts)	Wavelength (microns)
	5000	448
	5250	406
space	5500	370
charge	6000	311
limited	6500	265
	7000	228
transition		
	7500	200
	8000	175
	8500	155
	9000	138
	9500	124
	10000	112
	10500	101

this approach is that the neutralization method also provides useful thrust. Although the development of positive colloid arrays are well-advanced, negative arrays are less developed at the present time. Another promising approach to beam neutralization involves the use of low voltage, electron field emission MEMs arrays. An alternative to these less well-developed methods are hot filaments that provide a source of thermionic electrons. Although there are a large number of different thermionic sources available[5], we have elected to study the neutralization performance of thoria-coated iridium filaments. Thoria-coated iridium filaments have the following advantages over other thermionic electron emissive devices:

1. Unlike some dispenser cathodes, no conditioning is required.
2. The low work function (˜2.7 eV) enables operation at lower temperature, hence lower power.
3. The filaments are chemically resistant to corrosive gases and water vapor.
4. Lifetimes of over 1000 hours have been reported where the emission current density is 0.2 A/cm^2 or lower[6].
5. The filaments resist burnout even at limited exposure to atmosphere while hot.

Because of these advantages and robustness, thoria-coated iridium filaments are widely used as cathodes in ion gauge tubes[7] and as filaments for mass spectrometers[8]. Additionally, these filaments are used as oxidation resistant cathodes to improve the operational-lifetime of Kaufman ion sources[6].

To simply measure the emission characteristics of the thoria-coated neutralizer filament, a one-inch long, 0.007 diameter coiled filament was mounted in a vacuum system directly opposite a collector plate. Electron currents collected by the plate were measured as a function of both the filament current and the positive voltage applied to the collector plate. The results are displayed in Fig.11 . Emission limited operation was not encountered over the range of collector voltages applied. The positive voltage applied to the collector plate simulates colloid beam operation where the positive beam potential attracts electrons from the filament into the beam. We anticipate that filament operation at 2.6 A or lower will be sufficient to match the positive emission from a linear slit or capillary array colloid microthruster.

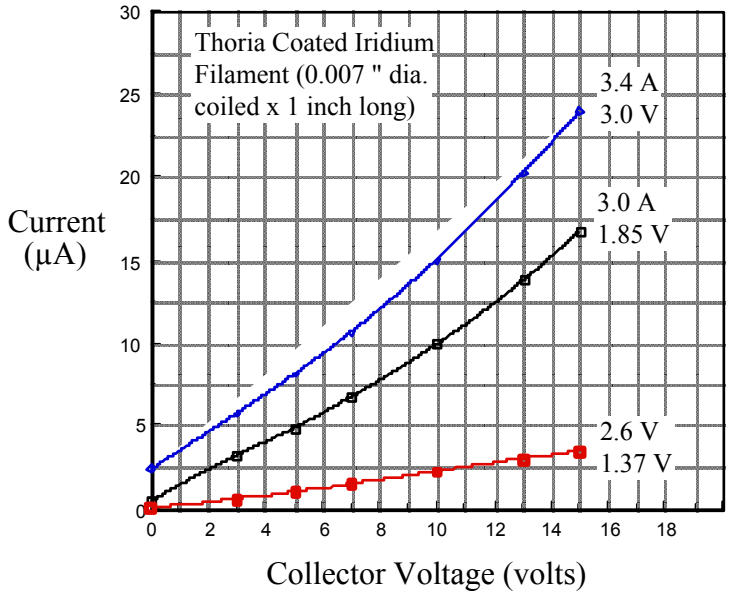

Fig. 11 Neutralizer performance.

Innovative Colloid Microthruster Design

Traditionally, colloid thrusters, based on capillary or linear slit designs, were fabricated using metallic materials. With the advent of microfabrication/MEMs technologies, materials such as Si and SiO_2, to name a few, are available for mass-producing microfluidic designs suitable for colloid microthruster fabrication. Since the benefits of integrating colloid microthruster development with microminiaturization technologies are many, we have been studying the colloid emission characteristics using single emitter, fused silica (SiO_2) capillary tubing. A conceptual view of a colloid microthruster using a linear array of multiple fused silica emitters is shown in Fig. 12. In this design, high voltage is applied to the propellant in the plenum housing. The emitting end of the fused silica is allowed to protrude a distance (see figure) equal to about one-half the capillary diameter (˜ 0.007-0.010 inch in single emitter tests). The plenum or emitter housing can be made from insulating materials but requires the insertion of a chemically inert (Au, Pt, e.g.) conducting electrode into the propellant plenum. In this case, a conducting electrolyte must be carefully chosen that does not generate non-soluble or gaseous by-products once electrons are transferred from the anions in solution to the electrode.

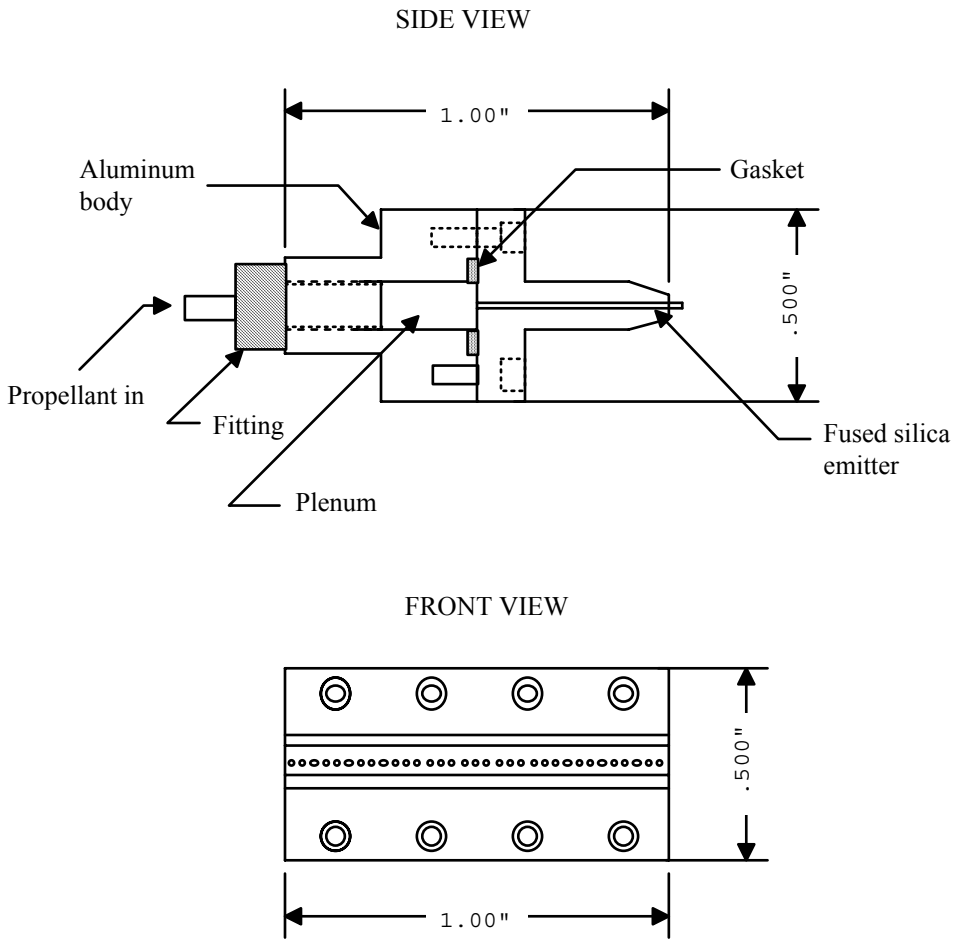

Fig. 12. Fused silica based colloid microthruster design (not to scale).

An advantage of the fused silica design is that charge transfer from the solution does not take place at the emission (high field) region eliminating the possibility of electrochemically activated deposits that could form at the solution/capillary interface, as in the case of metallic emitters. Furthermore, the emission characteristics at the tip are not dependent on the wetting conditions (which can vary) encountered with metal capillaries. Another benefit of using silica capillaries derives from the non-dependence on rim thickness and uniformity inherent in metal capillaries. By eliminating metal capillaries made from platinum or platinum alloys necessary to prevent electrochemical corrosion, expenses associated with emitter fabrication are greatly reduced. We have found that in single emitter tests, that fused silica emitters are surprisingly robust and resistant to corrosion. As an alternative to glycerol-based propellants, we are presently studying 80-90% aqueous based propellants using silica capillary emitters.

References

[1] P.W. Kidd, "Parametric studies of a single needle colloid thruster", AIAA Paper No. 67-530, *AIAA Electric Propulsion and Plasmadynamics Conf.,* Colorado Springs, CO., Sept. 11-13, 1967.

[2] J. Perel, J.F. Mahoney and H.L. Daley, "Duration test of an annular colloid thruster*", AIAA 9th Electrical Propulsion Conference*, Bethesda, MD, April 17-19, 1972.

[3] M.N. Huberman and E. Cohen, "Research on charged particle electrostatic thrusters", *Technical Report AFAPL-TR-67-115*, September 19667.

[4] L.D. Landau, E.M. Lifshitz and L.P. Pitaevskii, *Electrohydrodynamics of Continuous Media*, Pergamon Press, New York, 1984. (See problem 5, p.33).

[5] G.A. Haas, "Thermionic Electron Sources", *NRL Report 5657*, Oct. 6, 1961.

[6] C. R .Guarnieri, K.V. Ramanathan, D.S. Yee, and J.J. Cuomo, "Improved Ion Source For Use With Oxygen", *J. Vac. Sci. Technol., A(6)*, 2582 (Jul/Aug 1988).

[7] W.H. Kohl, *Handbook of Materials and Techniques For Vacuum Devices*, Reinhold Publishing Corp, New York, NY, 1967.

[8] C.E. Melton, "Application of Thoria-Iridium as the Source of Ionizing Electrons in Mass Spectrometry", *Rev. Sci. Instrum*., 29, 250 (Mar. 1958).